Title

New Insights into Secondary Organic Aerosol Formation at the Air—Liquid Interface

Journal

The Journal of Physical Chemistry Letters, 12(1)

ISSN

1948-7185

Authors

Sui, Xiao

Xu, Bo

Yao, Jenn

et al.

Publication Date

2021-01-14

DOI

10.1021/acs.jpclett.0c03319

Peer reviewed

New Insights into secondary organic aerosol formation at the air – liquid interface

Xiao Sui,[‡, †, *] Bo Xu,[‖] Jenn Yao,[†] Oleg Kostko,[‖] Musahid Ahmed,[‖] and Xiao-Ying Yu[†, *]

[‡] College of Geography and Environment, Shandong Normal University, Jinan, 250358, China

[†] Energy and Environment Directorate, Pacific Northwest National Laboratory, Richland, WA, 99354.

[‖] Chemical Sciences Division, Lawrence Berkeley National Laboratory, Berkeley, CA. 94720, USA

Supporting Information Placeholder

ABSTRACT: Air – liquid interfacial processing of volatile organic compound photooxidation has been suggested as an important source of secondary organic aerosols. However, owing to the lack of techniques for studying the air – liquid interface, the detailed interfacial mechanism remains speculative. To obviate this, we enabled in situ liquid synchrotron-based vacuum ultraviolet single photon ionization mass spectrometry using the system for analysis at the liquid – vacuum interface microreactor to study glyoxal photooxidation at the air – liquid interface. Determination of reaction intermediates and new oxidation products, including polymers and oligomers, by mass spectral analysis and appearance energy measurements has been reported for the first time. Furthermore, an expanded reaction mechanism of photooxidation and free radical induced reactions as a source of aqueous secondary organic aerosol formation is proposed. Single photon ionization can provide new insights into interfacial chemistry involving liquid as a condensed phase.

TOC Graphic

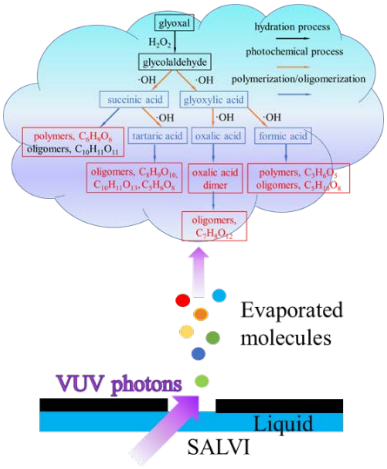

Key Words

aqueous secondary organic aerosol, glyoxal, photooxidation mechanism, air – liquid interface, single photon ionization mass spectrometry, dissociative photoionization.

Secondary organic aerosol (SOAs) are recognized as a main source of the earth atmospheric compositional change due to industrialization in recent human history and they directly affect global climate, human health, and the environment. Although interfacial reactions are speculated as a source of SOA, little is known due to the difficulty in studying interfaces using existing techniques.[1-2] The air – liquid (a – l) interfacial uptake of volatile organic compounds (VOCs), such as glyoxal and aldehydes, could generate aqueous secondary organic aerosols (aqSOAs)[3] and lead to high SOA budget.[4-5] However, large uncertainties of SOA formation exist at the a – l interface because of lack of suitable in situ techniques to probe reaction products.[6]

Synchrotron based single-photon ionization mass spectrometry (SPI-MS) using bright vacuum ultraviolet (VUV) photons is considered a "soft" and efficient way to study organic molecules susceptible to fragmentation.[7] It has been widely used in complex chemical systems to detect organic molecules with fewer fragments compared to traditional harsh ionization methods, such as electron impact, and allows for determination of ionization energies (IEs) which aids in chemical identification and isomer selectivity.[8] Coupling VUV radiation with mass spectrometry is regarded as a traditional gas phase and gas – solid interfacial experiment, because measurements must be performed under high vacuum.[9-10] Nevertheless, recent studies show that integrating a vacuum compatible microreactor, namely system for analysis at the liquid – vacuum interface (SALVI) [11-14] and VUV SPI-MS, makes it possible to study aqueous reactions in a dynamic environment.[15-16]

We present the combination of tunable synchrotron VUV SPI-MS and SALVI microreactor to observe molecular intermediates and products of glyoxal photooxidation at the a – l interface approximated by the liquid – vacuum interface in this work.[17-18] This *in situ* study of a – l interfacial SOA formation from photochemical oxidation using liquid VUV SPI-MS is the first to the best of our knowledge. Key products and reactants are identified using mass spectral analyses; and appearance energies (AEs) of these ions are determined. This approach broadens the application of traditional vacuum instrumentation typically limited to the gas and solid phase. Our results provide new understanding of the photochemical mechanism of importance in aqSOA formation affecting the global SOA budget. Moreover, we provide a new pathway to investigate a – l interfacial reactions that occur at material interfaces involving liquid as the condensed phase.

Figure 1 shows the schematic of the experimental setup and types of measurements using in situ liquid VUV SPI-MS. More details were reported recently[15-16] and in the Supporting Information (SI). Briefly, liquid consisting of glyoxal and hydrogen peroxide was sealed in between two silicon nitride membranes in the microchannel of SALVI (Fig. 1b), and the liquid was withheld by its surface tension across the aperture in high vacuum.[11-14] Two micrometer-sized apertures were milled to allow liquid evaporation, making it possible to detect evaporated molecules during experiments in high vacuum (Figs. 1c-1d). Table S1 lists the aqueous samples investigated in this work. Interferences that may occur from components of the SALVI device consisting of polydimethylsiloxane (PDMS) are evaluated prior to peak analysis. Approximately 2.6% of total counts are from the PDMS interference peaks, indicating that their contributions are insignificant (Table S2). Furthermore, the glyoxal control sample (i.e., without hydrogen peroxide (H_2O_2) and UV treatment) was studied and its mass spectrum included for spectral comparison.

Figures 2 and S1 depict mass spectral comparison of UV aged samples consisting of glyoxal and H_2O_2 as well as the glyoxal control measured at different photon energies. Glyoxal is mainly observed as dissociative fragments, such as m/z 45, CHO_2^+, m/z 75, $C_2H_3O_3^+$, m/z 91 $C_2H_3O_4^+$, and m/z 106 $C_3H_6O_4^+$, from glyoxal or its dimer ions (i.e., m/z 116 and 130) [19] at the aqueous surface (shown in Figs. 2 and S1). The glyoxal-related fragments peaks of

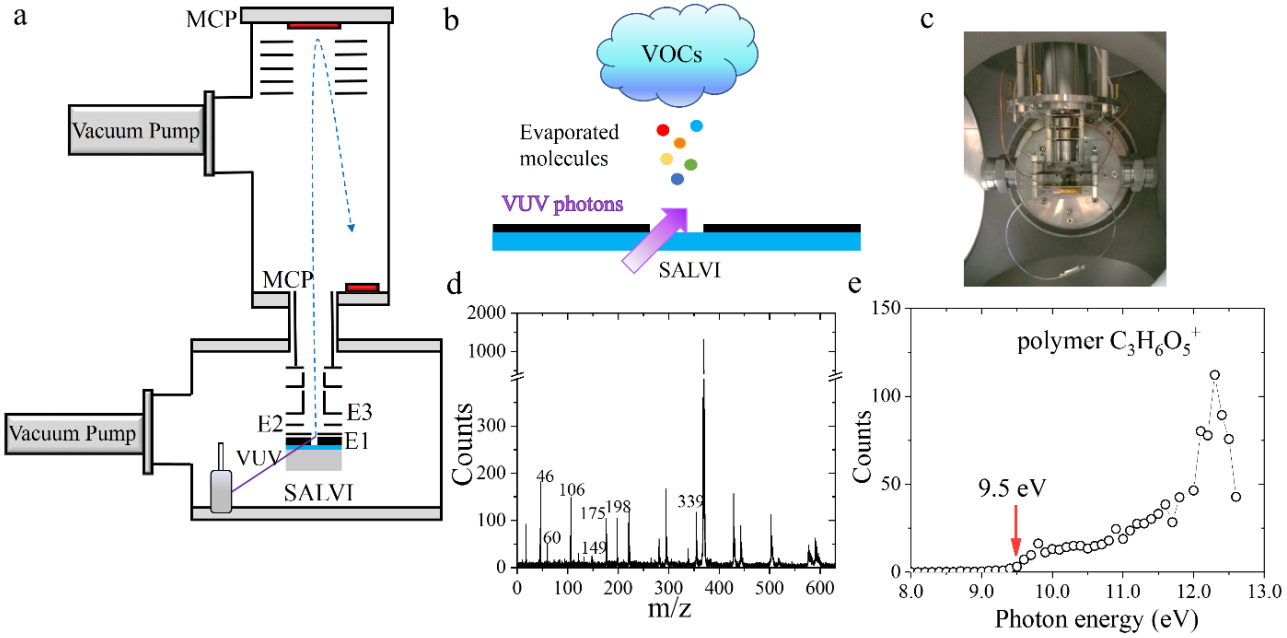

Figure 1. The SALVI device integrated into the VUV photoionization mass spectrometer. a) The electrode in the ion optics of Reflectron time-of-flight mass spectrometry (Re ToF-MS) with the attached SALVI device; b) the schematic showing the relative position of the photon flux and the aperture of the SALVI microchannel; c) a photo showing the integration inside the chamber; d) a mass spectrum of the 4 hr. UV aged sample obtained at photon energy of 10.7 eV; and e) a photoionization efficiency plot of $C_3H_6O_5^+$. The schematic diagram in (a) was adapted from Komorek et al., 2018.[16]

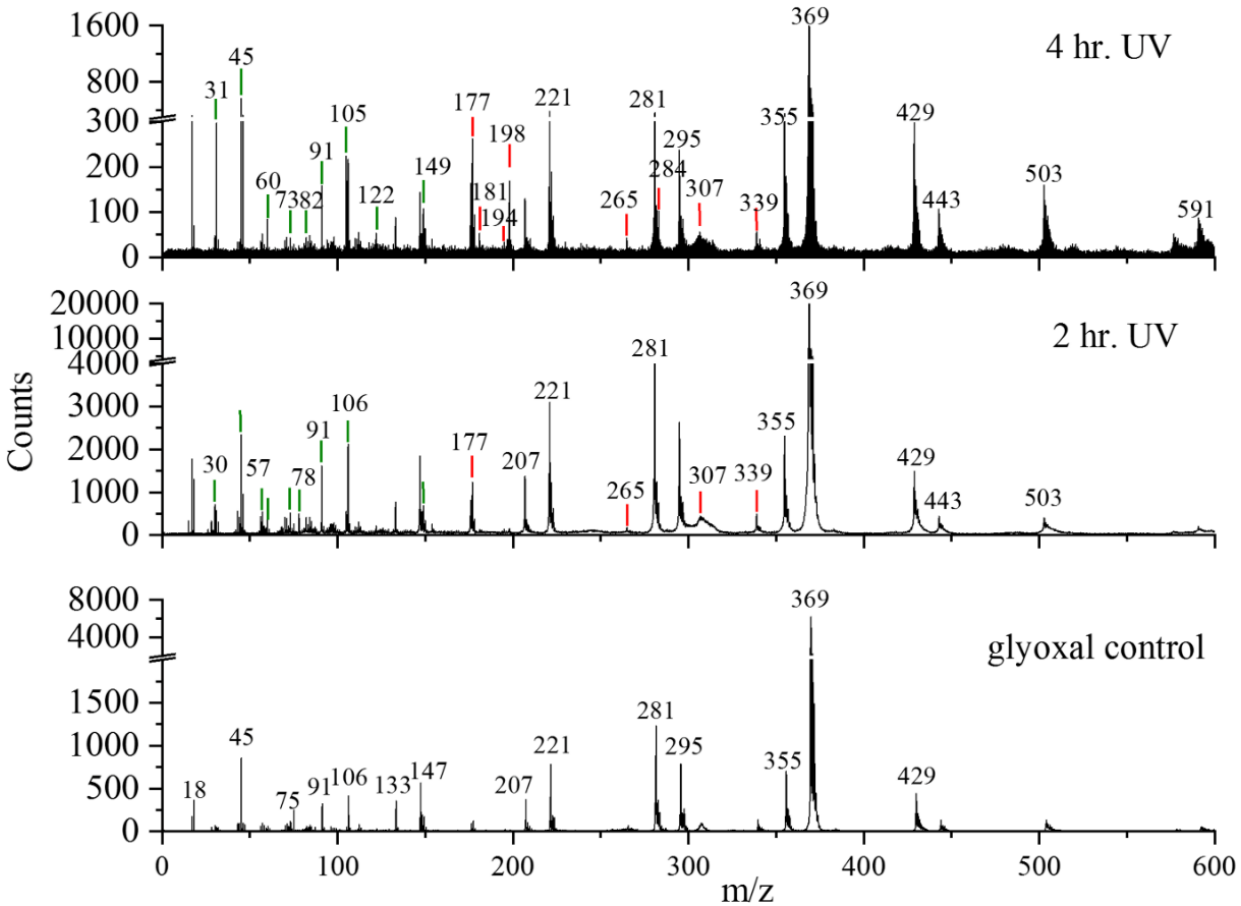

Figure 2. VUV SPI-MS spectral comparison of the glyoxal control, 2 hr., and 4 hr. photochemical aging of glyoxal and hydrogen peroxide solutions acquired at photon energy of 12.0 eV. Green drop lines stand for reactant, intermediates, and products such as carboxylic acids; and red drop lines polymers/oligomers in UV aged samples. Peaks from glyoxal control and PDMS are marked without drop lines.

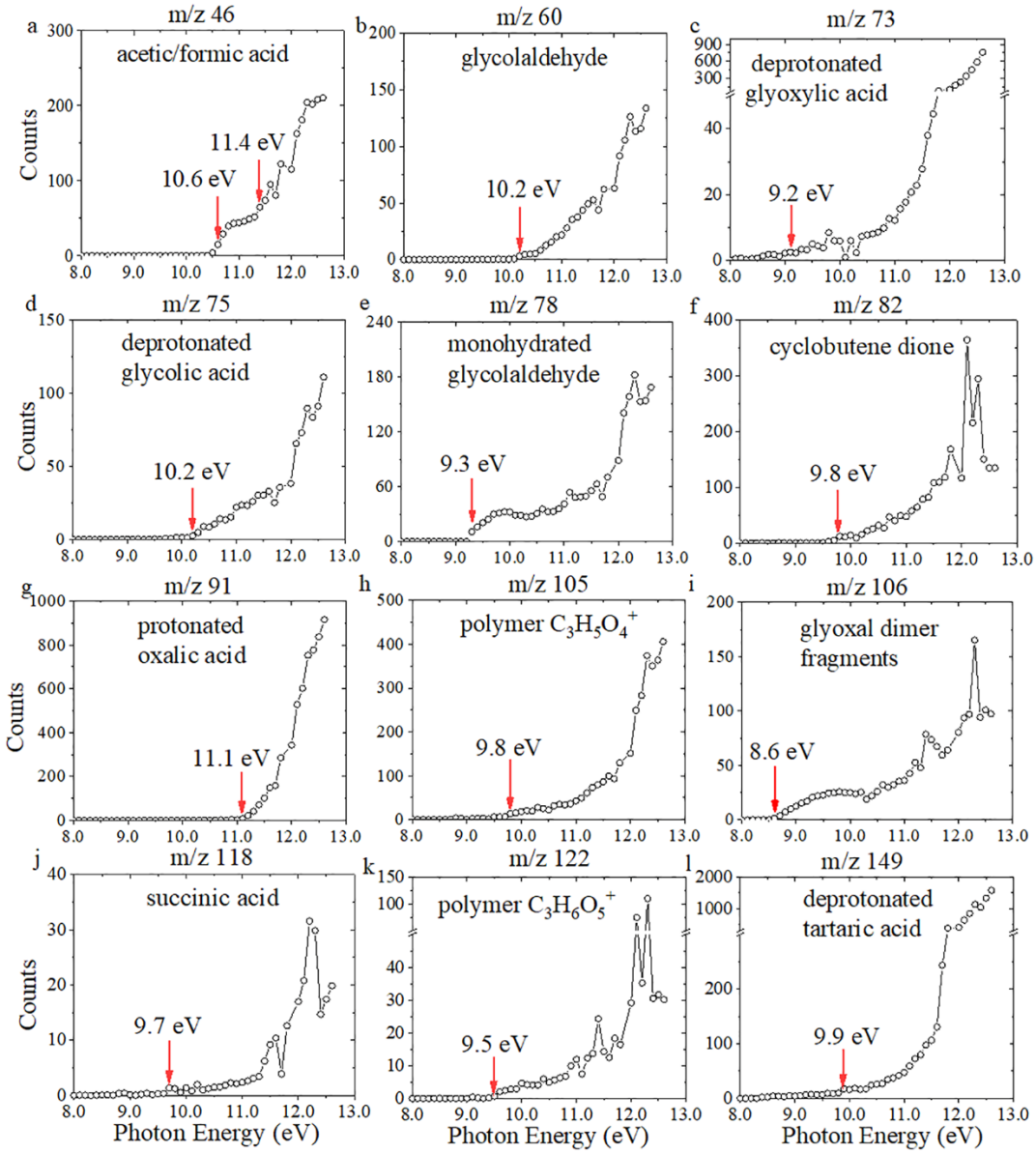

Figure 3. PIE curves and appearance energies (AEs) of key products from the 2 hr. UV aging observations. Red arrows indicate AEs.

m/z 45, 75, 91, and 106 are observed in the 1 hr. sample at photon energy of 10.7 eV and is shown in Fig. S1, while the 2 hr. and 4 hr. UV processed samples are measured at 12.0 eV, as seen in Fig. 2. A number of product peaks are detected in the samples after 1 hr., 2 hr., and 4 hr. UV aging, respectively, when compared against the glyoxal control. The mass spectral comparison shows that photochemical oxidation products indeed form at the a – l interface as a result of glyoxal UV aging.

The ion counts of the 2 hr. and 4 hr. samples were affected by the optical alignment of the device relative to the photon beam and the instrument parameter differences between experimental runs and beamline visits. It should be possible to perform quantitative analysis using optimized instrumental setup in the future. The mass spectra contain information of ions both from neutral and dissociative photoionization molecules.[20] Identifications of key reactants and products are summarized in Table 1. Peak identification was performed based on existing knowledge of the glyoxal oxidation reported in previous findings. Further, published IE values are another source to unambiguously determine a species. During TOF mass extraction, a continuous wave ion beam is converted to a pulsed beam. Pulsing affects the mass spectra dramatically and the resolution is not uniform over the mass range. However, peak separation is not a problem; generally peak positions can be identified to two decimal places of accuracy as shown in Fig. S2. The molecules with relative high vapor pressures, such as aldehyde and carboxylic acid with small molecular weight (e.g., m/z < 400), were detected with higher counts. However, complex oligomers has relative lower intensities in the mass spectra partially due to their lower vapor pressure (also shown in Fig. 2). The glyoxal oxidation products can dissociate to smaller fragments, namely CH_2O^+ m/z 30, CH_2OH^+ m/z 31, and $CHOCO^+$ m/z 57 at a higher photon energy of 12.0 eV. Neutral carboxylic acids derived from glyoxal oxidation by hydroxyl radicals (•OH) are detected as their respective parent ions as expected, such as formic acid m/z 46 and succinic acid m/z 118. Some carboxylic acids are mainly observed as deprotonated fragments at higher photon energies as shown in Fig. S2, for instance, glyoxylic acid m/z 73, glycolic acid m/z 75, and tartaric acid m/z 149. Important intermediates, such as glycolaldehyde m/z 60 and monohydrated glycolaldehyde m/z 78 ions, are representative of neutral molecules in the reactions. Furthermore, newly discovered molecules and/or dissociated products, including m/z 82 $C_4H_2O_2^+$, m/z 122 $C_3H_6O_5^+$, m/z 181 $C_4H_5O_8^+$, m/z 194 $C_5H_6O_8^+$, m/z 198 $C_5H_{10}O_8^+$, m/z 265, $C_8H_9O_{10}^+$, m/z 284 $C_7H_8O_{12}^+$, m/z 307 $C_{10}H_{11}O_{11}^+$, and m/z 339 $C_{10}H_{11}O_{13}^+$ (see Fig. 2 and Table 1), are observed at the a – l interface at the photon energy of 12.0 eV.

Overall, carboxylic acids, an important glyoxal photochemical aging products, are found in all UV aged samples.

Larger organic molecules, including polymers and oligomers, also form after several hours of photochemical processing. This finding is consistent with our recent *in situ* studies conducted using liquid time-of-flight secondary ion mass spectrometry (ToF-SIMS) at the a – l interface,[17-18] confirming that liquid VUV SPI-MS is a viable approach for probing interfacial reactions involving the liquid phase.

The ionization energy of a molecule is a significant parameter inherent of chemical species and structures.[21] A photoionization efficiency curve (PIE) obtained by integrating ion intensity at each photon energy can be used to determine an experimental appearance energy and can be compared with known ionization energies to infer chemical identification and isomer selectivity.[20] Complex intermediates and oxidation products are discovered in the glyoxal a – l interfacial reactions, different from the bulk analysis.[19, 22] Thus, it is advantageous to identify the photooxidation products unambiguously according to their AEs. AE values obtained in this work are summarized in Table 1. The AE values are mainly determined as the first photon energy at the point where a steady increase from baseline is observed.[23] The observed AEs of main fragments from the glyoxal control sample are shown on top of the PIE curves in Fig. S3. PIE curves derived from the photon energies scanned between 8.0 to 12.6 eV at 0.1 eV step of the 2 hr. UV aged sample are illustrated in Figs. 3 and S4. Additionally, AEs derived from the 4 hr. UV aging observations are depicted in Fig. S5, showing that aging time has no effects on AEs as anticipated.

Table 1. Peak Identification and Determination of Appearance Energies of Key Reactants and Products in the Positive Mode

m/z, obs[a]	m/z, the[b]	Formula	Chemical Name	AE	Reference
46	46.03	$CH_2O_2^+$	acetic acid/formic acid	10.6, 11.4	17-18, 23
60	60.05	$C_2H_4O_2^+$	glycolaldehyde	10.2	17, 18
73	73.07	$C_3H_5O_2^+$	deprotonated glyoxylic acid	9.2	24
75	75.04	$C_2H_3O_3^+$	deprotonated glycolic acid	10.2	24
78	78.07	$C_2H_6O_3^+$	monohydrated glycolaldehyde	9.3	17, 18,
82	82.06	$C_4H_2O_2^+$	cyclobutene dione	9.8	25
91	91.04	$C_2H_3O_4^+$	protonated oxalic acid	11.1	17, 18
105	105.07	$C_3H_5O_4^+$	polymer	9.8	17, 18
106	106.08	$C_3H_6O_4^+$	glyoxal dimer fragment	8.6[c]	This work
118	118.13	$C_5H_{10}O_3^+$	succinic acid	9.7	17, 18
122	122.08	$C_3H_6O_5^+$	polymer	9.5[c]	This work
149	149.08	$C_4H_5O_6^+$	deprotonated tartaric acid	9.9	17, 18
177	177.13	$C_6H_9O_6^+$	polymer	10.1[c]	This work
181	181.08	$C_4H_5O_8^+$	protonated oxalic acid dimer	9.6[c]	This work
194	194.14	$C_5H_6O_8^+$	polymer	9.7[c]	This work
198	198.13	$C_5H_{10}O_8^+$	oligomer	8.8[c]	This work
265	265.15	$C_8H_9O_{10}^+$	oligomer	9.8[c]	This work
284	284.13	$C_7H_8O_{12}^+$	oligomer	9.0[c]	This work
307	307.23	$C_{10}H_{11}O_{11}^+$	oligomer	9.7	26
339	339.19	$C_{10}H_{11}O_{13}^+$	oligomer	9.7[c]	This work

[a] observed m/z in this experiment
[b] theoretical m/z
[c] AE values determined in this work

First, we study glyoxal, carboxylic acids, and several key photochemical products of interfacial photo-oxidation using their PIE curves as shown in Fig. 3, while additional details of intermediates and polymers are reported in the SI (Figs. S4 – S5). The PIE curve of m/z 46 (Fig. 3a) suggests that two chemical compounds are ionized with different photon energies at 10.6 eV and 11.4 eV, respectively. These two products are assigned as fragments of acetic acid and formic acid by comparing with IEs determined previously.[23] The AEs for deprotonated glyoxylic acid (m/z 73, Fig. 3c) and deprotonated glycolic acid (m/z 75, Fig. 3d) are 9.2 eV and 10.2 eV, respectively. The AE for product m/z 82 (Fig. 3f) is 9.8 eV, and it is assigned as cyclobutene dione referencing to the known IE.[25] The PIE curve of m/z 91 (Fig. 3g) has an AE of 11.1 eV, which is identified as protonated oxalic acid. The AE for m/z 106 of 8.6 eV (Figs. 3i and S3d) is suggested as the glyoxal dimer fragment $C_3H_6O_4^+$. Additionally, the AEs for succinic acid m/z 118 (Fig. 3j) and deprotonated tartaric acid m/z 149 (Fig. 3l) are determined as 9.7 eV and 9.9 eV, respectively Molecules with carboxyl groups have higher AEs, for instance, formic acid 11.4 eV and oxalic acid 11.1 eV. In contrast, the AEs for molecules with hydroxyl acid functional groups have AE values close to 10.0 eV.

Furthermore, the AEs of intermediates and oxidation products including polymers and oligomers from glyoxal photochemical a – l interfacial reactions are reported. The AEs of reaction intermediates, including glycolaldehyde m/z 60 (Fig. 3b) and monohydrated glycolaldehyde m/z 78 (Fig. 3e) are determined to be 10.2 eV and 9.3 eV, respectively. Additional AEs of polymer and oligomers formed at the a – l interface are shown as the following: m/z 105 $C_3H_5O_4^+$ 9.8 eV (Fig. 3h), m/z 122 $C_3H_6O_5^+$ 9.5 eV (Fig. 3k), m/z 177 $C_6H_9O_6^+$ 10.1 eV (Fig. S4a), m/z 181, $C_4H_5O_8^+$ 9.6 eV (Fig. S4b), m/z 194 $C_5H_6O_8^+$ 9.7 eV (Fig. S4c), m/z 198 $C_5H_{10}O_8^+$ 8.8 eV (Fig. S4d), m/z 265 $C_8H_9O_{10}^+$ 9.8 eV (Fig. S4e), m/z 284 $C_7H_8O_{12}^+$ at 9.0 eV (Fig. S4f), m/z 307 $C_{10}H_{11}O_{11}^+$ at 9.7 eV (Fig. S4g), and m/z 339 ($C_{10}H_{11}O_{13}^+$) at 9.7 eV (Fig. S4h). It is worth noting that many oligomers have similar AEs, ranging from 9.5 to 10.1 eV, which implies that they share the same functional groups (e.g., hydroxyl, carboxyl, ester). However, the AEs of m/z 198 $C_5H_{10}O_8^+$ and m/z 284 $C_7H_8O_{12}^+$ are close to 9.0 eV, suggesting

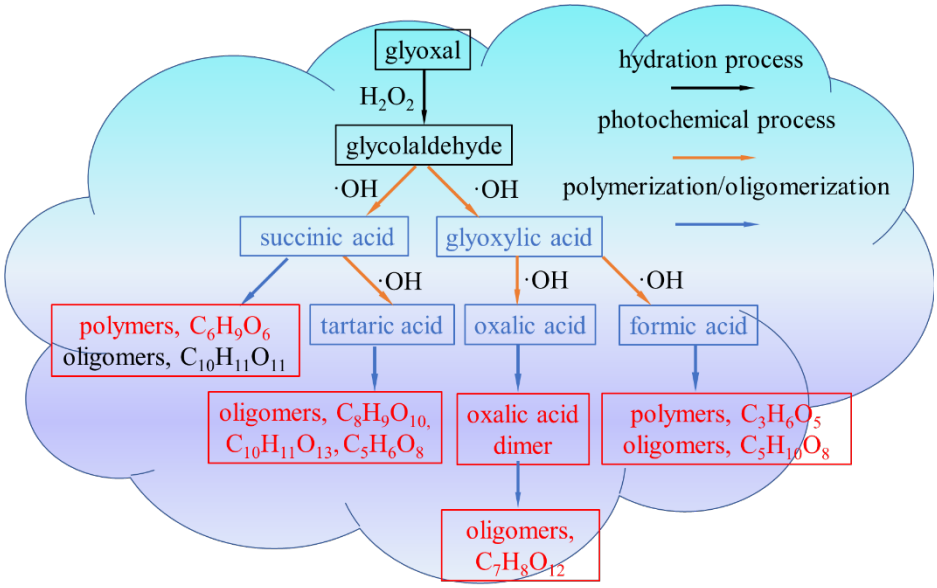

Figure 4. The expanded secondary organic aerosol reaction flow chart of glyoxal photochemical reactions based on in situ liquid VUV SPI-MS results. Black color represents hydration process, orange photochemical process, and blue polymerization/oligomerization. Blue font and boxes are known carboxylic acids and red representative new products.

that the structures of those oligomers are different (as shown in Scheme S1). The multistep increments of PIEs suggested there might be more than one functional group in these oligomers. These results indicate that the uptake of VOCs at the a – l interface could be explored using the synchrotron VUV SPI-MS and interfacial products can be determined based on m/z values and AEs. Glycolaldehyde was regarded as a reactant that can produce glyoxal in the gas phase.[27] However, glycolaldehyde at the a – l interface is observed as a hydration product as a result of the glyoxal UV photochemical reactions.[17] Glycolic acid could form via aldehyde reactions with •OH as a new pathway for carboxylic acids at the a – l interface, because glyoxylic acid and oxalic acid are produced as a result of glyoxylic acid photooxidation. These results are consistent with those from bulk experiments.[28] The peak intensity of formic acid in the 4 hr. UV sample is higher than other samples, which indicates that formic acid is likely to be a multiple generation product from glyoxylic acid or glyoxal decomposition due to continuous reactions instead of direct production from glyoxal.[22] Another formation pathway of organic acids is that larger products could form via radical – radical reactions, for instance, succinic and tartaric acid in the presence of aldehyde and peroxy radical.[28-29] The mass spectral analysis suggests that the formation of larger organic acids may be due to ongoing UV reactions after several hours at the a – l surface. The subsequent reaction products are organic polymers and oligomers, which are identified as an important source of SOAs via aqueous chemistry.[30] Oligomer formation is facilitated by longer photochemical processing time; more peaks with higher intensity are observed in the 2 hr. and 4 hr. UV aged samples (Figs. 2 and S1).

Our new *in situ* liquid VUV SPI-MS results demonstrate that several pathways could lead to aqSOA formation at the a – l interface. Specifically, oxalic acid could form dimers by hydrogen bonding [31] and oligomerization (e.g., newly discovered high mass products m/z 181, $C_4H_5O_8^+$ and m/z 284, $C_7H_8O_{12}^+$ in Fig. 2 and Table 1). We suggest that formic acid contribute to the SOA budget by forming •COOH and •HCOO via photochemical reactions, providing direct evidence as speculated earlier.[32] Furthermore, we propose that formic acid is likely to participate in oligomer formation (i.e., $C_3H_6O_5$, $C_5H_{10}O_8$) by esterification or radical reaction (Table S3 and Scheme S1). Succinic acid and tartaric acid are related to oligomer formation, and they mainly form after several hours of UV aging. Additionally, a new pathway for succinic acid to contribute to aqSOA formation is proposed, that is, succinic acid could form larger products (i.e., $C_6H_9O_6$, $C_{10}H_{11}O_{11}$) by acid catalysis or radical reactions. Tartaric acid may also participate in the production of oligomers via esterification, oligomerization, or radical reaction, for example, $C_8H_9O_{10}$, $C_{10}H_{11}O_{13}$, and $C_5H_6O_8$. There is no direct evidence that cyclobutene dione could be generated from glyoxal oxidation. Thus, this product likely arises from the dissociated cyclic oligomers formed by hemiacetal.[29] The expanded reaction flowchart is depicted in Fig. 4 with new products discovered in this study highlighted in red. Suggested structures and reaction pathways of representative new compounds are presented in Table S3 and Scheme S1.

In summary, synchrotron-based in situ liquid VUV SPI-MS has been first enabled to study a – l interfacial reactions in a microfluidic reactor to deepen the understanding of aqSOA formation. VUV photons offer a unique opportunity to study interfacial reactions and dynamics of soluble VOCs that exist in the atmosphere via the determination provide new pathways to determine the chemical structures of key products by their appearance energies, providing more scientific insights into the aqSOA formation mechanism. This work sets the foundation of in operando kinetic studies of a – l interfacial studies to capture formation of radicals, transient species, and oligomers in action involving the liquid condensed phase and opens a new realm of applications of instruments traditionally limited to solid and gas analyses in vacuum.

ASSOCIATED CONTENT

Supporting Information

Additional experimental details and theoretical results in PDF are provided in Supporting Information.

AUTHOR INFORMATION

Corresponding Authors

Corresponding author

Dr. Xiao-Ying Yu – Energy and Environment Directorate, Pacific Northwest National Laboratory, Richland, Washington 99354, United States; ORCID: 0000-0002-9861-3109; Tel: (1) 509-372-4524; E-mail: xiaoying.yu@pnnl.gov.

Authors

Dr. Xiao Sui –College of Geography and Environment, Shandong Normal University, Shandong Province Jinan, 250358, China; Energy and Environment Directorate, Pacific Northwest National Laboratory, Richland, WA 99354, USA. ORCID: 0000-0002-4371-6178
Dr. Bo Xu – Chemical Sciences Division, Lawrence Berkeley National Laboratory, Berkeley, CA. 94720, USA. ORCID: 0000-0002-1120-3423
Ms. Jenn Yao – Energy and Environment Directorate, Pacific Northwest National Laboratory, Richland, WA 99354, USA. ORCID: 0000-0001-7349-0678
Dr. Oleg Kostko – Chemical Sciences Division, Lawrence Berkeley National Laboratory, Berkeley, CA. 94720, USA. ORCID: 0000-0003-2068-4991
Dr. Musahid Ahmed – Chemical Sciences Division, Lawrence Berkeley National Laboratory, Berkeley, CA. 94720, USA. ORCID: 0000-0003-1216-673X

Author Contributions

XYY designed the experiments. XS, XYY, OK, and MA wrote the paper. BX, XYY, and JY performed the experiments. XS, BX, OK, MA, and XYY did analysis. All authors have given approval to the final version of this manuscript.

Notes

The authors declared no competing interests.

ACKNOWLEDGMENTS

XS is grateful for the support from Pacific Northwest National Laboratory (PNNL) Alternate Sponsored Fellowship (ASF). X-Y Y and JY were grateful for the support from the PNNL Earth and Biological Science Directorate (EBSD) mission seed Laboratory Directed Research and Development (LDRD) support to perform beamline experiments. X-Y Y thanks Office of Science, Office of Basic Energy Sciences, of the U.S. DOE through the Direct Air Capture Program for partial support in writing this manuscript. This research used resources of the Advanced Light Source, a Department of Energy (DOE) Office of Science User Facility under contract no. DE-AC02-05CH11231. BX, OK, and MA are supported by the Director, Office of Science, Office of Basic Energy Sciences, of the U.S. DOE under Contract No. DE-AC02-05CH11231, through the Gas Phase Chemical Physics Program and Condensed Phase, Interfaces, and Molecular Sciences Program. PNNL is operated for the U.S. DOE by Battelle Memorial Institute under Contract No. DE-AC05-76RL01830. The authors thank Miss Rachel Komorek, Dr. Fei Zhang, Dr. Jiachao Yu, and Dr. Tyler Troy for device fabrication, sample preparation, and experimental assistance.

References

1. Zhang, R.; Wang, G.; Guo, S.; Zamora, M. L.; Ying, Q.; Lin, Y.; Wang, W.; Hu, M.; Wang, Y. Formation of urban fine particulate matter. *Chem. Rev.* **2015,** *115* (10), 3803-55.

2. Ji, Y.; Shi, Q. L.; An, Y.; Zheng, T.; Peng, J.; Gao, J.; Chen, Y.; Li, J.; Wang, G.; Zhang, Y. et al. Carbenium ion-mediated oligomerization of methylglyoxal for secondary organic aerosol formation. *Proc. Natl. Acad. Sci.* **2020,** *117* (24), 13294-13299.

3. Gilardoni, S.; Massoli, P.; Paglione, M.; Giulianelli, L.; Carbone, C.; Rinaldi, M.; Decesari, S.; Sandrini, S.; Costabile, F.; Gobbi, G. P. et al. Direct observation of aqueous secondary organic aerosol from biomass-burning emissions. *Proc. Natl. Acad. Sci.* **2016,** *113* (36), 10013-10018.

4. McNeill, V. F. Aqueous organic chemistry in the atmosphere: sources and chemical processing of organic aerosols. *Environ. Sci. Technol.* **2015,** *49* (3), 1237-44.

5. Garrett, B. C. Ions at the air/water interface. *Science* **2004,** *303* (5661), 1146-1147.

6. Yu, X. Y.; Liu, B. W.; Yang, L. Imaging liquids using microfluidic cells. *Microfluid. Nanofluid.* **2013,** *15* (6), 725-744.

7. Gasper, G. L.; Takahashi, L. K.; Zhou, J.; Ahmed, M.; Moore, J. F.; Hanley, L. Laser Desorption Postionization Mass Spectrometry of Antibiotic-Treated Bacterial Biofilms Using Tunable Vacuum Ultraviolet Radiation. *Anal. Chem.* **2010,** *82*, 7472–7478.

8. Kostko, O.; Bandyopadhyay, B.; Ahmed, M. Vacuum Ultraviolet Photoionization of Complex Chemical Systems. *Annu. Rev. Phys. Chem.* **2016,** *67*, 19-40.

9. Ahmed, M.; Kostko, O. From atoms to aerosols: probing clusters and nanoparticles with synchrotron based mass spectrometry and X-ray spectroscopy. *Phys. Chem. Chem. Phys.* **2020,** *22* (5), 2713-2737.

10. Zhao, L.; Kaiser, R. I.; Lu, W.; Xu, B.; Ahmed, M.; Morozov, A. N.; Mebel, A. M.; Howlader, A. H.; Wnuk, S. F. Molecular mass growth through ring expansion in polycyclic aromatic hydrocarbons via radical–radical reactions. *Nat. Commun.* **2019,** *10* (1), art. no. 3689.

11. Yang, L.; Yu, X. Y.; Zhu, Z. H.; Iedema, M. J.; Cowin, J. P. Probing liquid surfaces under vacuum using SEM and ToF-SIMS. *Lab Chip* **2011,** *11* (15), 2481-2484.

12. Yang, L.; Yu, X. Y.; Zhu, Z. H.; Thevuthasan, T.; Cowin, J. P. Making a hybrid microfluidic platform compatible for in situ imaging by vacuum-based techniques. *J. Vac. Sci. Technol. A* **2011,** *29* (6), art. no. 061101.

13. Liu, B.; Yu, X. Y.; Zhu, Z.; Hua, X.; Yang, L.; Wang, Z. In situ chemical probing of the electrode-electrolyte interface by ToF-SIMS. *Lab Chip* **2014,** *14*, 855-859.

14. Yu, J. C.; Zhou, Y. F.; Hua, X.; Liu, S. Q.; Zhu, Z. H.; Yu, X. Y. Capturing the transient species at the electrode-electrolyte interface by in situ dynamic molecular imaging. *Chem Commun* **2016,** *52* (73), 10952-10955.

15. Komorek, R.; Xu, B.; Yao, J.; Kostko, O.; Ahmed, M.; Yu, X. Y. Probing sulphur clusters in a microfluidic electrochemical cell with synchrotron-based photoionization mass spectrometry. *Phys. Chem. Chem. Phys.* **2020,** *22* (26), 14449-14453.

16. Komorek, R.; Xu, B.; Yao, J.; Ablikim, U.; Troy, T. P.; Kostko, O.; Ahmed, M.; Yu, X. Y. Enabling liquid vapor analysis using synchrotron VUV single photon ionization mass spectrometry with a microfluidic interface. *Rev.Sci. Instrum.* **2018,** *89* (11), 115105.

17. Sui, X.; Zhou, Y. F.; Zhang, F.; Chen, J. M.; Zhu, Z. H.; Yu, X. Y. Deciphering the aqueous chemistry of glyoxal oxidation with hydrogen peroxide using molecular imaging. *Phys. Chem. Chem. Phys.* **2017,** *19* (31), 20357-20366.

18. Zhang, F.; Yu, X.; Sui, X.; Chen, J.; Zhu, Z.; Yu, X. Y. Evolution of aqSOA from the Air-Liquid Interfacial Photochemistry of Glyoxal and Hydroxyl Radicals. *Environ. Sci. Technol.* **2019,** *53* (17), 10236-10245.

19. Carlton, A. G.; Turpin, B. J.; Altieri, K. E.; Seitzinger, S.; Reff, A.; Lim, H.-J.; Ervens, B. Atmospheric oxalic acid and SOA production from glyoxal: Results of aqueous photooxidation experiments. *Atmos. Environ.* **2007,** *41* (35), 7588-7602.

20. Mysak, E. R.; Wilson, K. R.; Jimenez-Cruz, M.; Ahmed, M.; Baer, T. Synchrotron radiation based aerosol time-of-flight mass spectrometry for organic constituents. *Anal. Chem.* **2005,** *77* (18), 5953-60.

21. Taatjes C. A.; McIlroy, N. H. A.; Miller, J. A.; Senosiain, J. P.; Klippenstein, S. J.; Qi, F.; Sheng, L.; Zhang, Y.; Cool, T. A.; Wang, J. et al. Enols Are Common Intermediates in Hydrocarbon Oxidation. *Science* **2005,** *308* (24), 1887-1889.

22. Lee, A. K.; Zhao, R.; Gao, S. S.; Abbatt, J. P. Aqueous-phase OH oxidation of glyoxal: application of a novel analytical approach employing aerosol mass spectrometry and complementary off-line techniques. *J. Phys. Chem. A* **2011,** *115* (38), 10517-26.

23. Pan, G.; Hu, C.; Huang, M.; Wang, Z.; Cheng, Y.; Liu, Z.; Gu, X.; Zhao, W.; Zhang, W.; Chen, J. et al. A VUV photoionization mass spectrometric study on the OH-initiated photooxidation of isoprene with synchrotron radiation. *J. Environ. Sci.* **2012,** *24* (12), 2075-2082.

24. Ervens, B.; Volkamer, R. Glyoxal processing by aerosol multiphase chemistry: towards a kinetic modeling framework of secondary organic aerosol formation in aqueous particles. *Atmos. Chem. Phys.* **2010,** *10* (17), 8219-8244.

25. Schang, P.; Gleiter, R.; Rieker, A. The He(I) Photoelectron Spectrum of Cyclobutene-l,2-dione and o-Benzoquinone. *Ber. Bunsen-Ges. Phys. Chem.* **1978,** *82*, 629-633.

26. Yi, T.; Perri, M. J.; Seitzinger, S. P.; Turpin, B. J. Effects of Precursor Concentration and Acidic Sulfate in Aqueous Glyoxal-OH Radical Oxidation and Implications for Secondary Organic Aerosol. *Environ. Sci. Technol.* **2009,** *43*, 8105–8112.

27. Warneck, P. In-cloud chemistry opens pathway to the formation of oxalic acid in the marine atmosphere. *Atmos. Environ.* **2003,** *37* (17), 2423-2427.

28. Perri, M. J.; Seitzinger, S.; Turpin, B. J. Secondary organic aerosol production from aqueous photooxidation of glycolaldehyde: Laboratory experiments. *Atmos. Environ.* **2009,** *43* (8), 1487-1497.

29. Lim, Y. B.; Tan, Y.; Perri, M. J.; Seitzinger, S. P.; Turpin, B. J. Aqueous chemistry and its role in secondary organic aerosol (SOA) formation. *Atmos. Chem. Phys.* **2010,** *10* (21), 10521-10539.

30. Mellouki, A.; Wallington, T. J.; Chen, J. Atmospheric chemistry of oxygenated volatile organic compounds: impacts on air quality and climate. *Chem. Rev.* **2015,** *115* (10), 3984-4014.

31. Mariusz P. Mitoraj, R. K., Marek Boczar, Artur Michalak. Theoretical description of hydrogen bonding in oxalic acid dimer and trimer based on the combined extended-transition-state energy decomposition analysis and natural orbitals for chemical valence (ETS-NOCV). *J. Mol. Model* **2010,** *16*, 1789–1795.

32. Paulot, F.; Wunch, D.; Crounse, J. D.; Toon, G. C.; Millet, D. B.; DeCarlo, P. F.; Vigouroux, C.; Deutscher, N. M.; González Abad, G.; Notholt, J. et al. Importance of secondary sources in the atmospheric budgets of formic and acetic acids. *Atmos. Chem. Phys.* **2011,** *11* (5), 1989-2013.